

Date of publication xxxx 00, 0000, date of current version xxxx 00, 0000.

Digital Object Identifier 10.1109/ACCESS.2024.0429000

# Design and Evaluation of a Lower Limb Orthoprostheses for Toddlers with Fibular Hemimelia Using Additive Manufacturing

LILLI ANDERS<sup>1</sup>, PAULA AGULHEIRO<sup>2</sup>, HUGO PLÁCIDO SILVA<sup>3,4,5</sup>, and CLAUDIA QUARESMA<sup>6,7</sup>.

<sup>1</sup>Department of Biomedical Engineering, Instituto Superior Técnico, University of Lisbon, Lisbon, 1949-001, Portugal

<sup>2</sup>Rehabilitation Center, Hospital Dona Estefânia, Centro Hospitalar Universitário de Lisboa Central (CHULC), 1169-050 Lisbon, Portugal

<sup>3</sup>Department of Bioengineering, Instituto Superior Técnico, University of Lisbon, Lisbon, 1949-001, Portugal; hsilva@lx.it.pt

<sup>4</sup>IT - Instituto de Telecomunicações, Instituto Superior Técnico, Lisbon, 1949-001, Portugal

<sup>5</sup>LUMLIS-Lisbon Unit for Learning and Intelligent Systems, Lisbon, 1049-001, Portugal

<sup>6</sup>Laboratório de Instrumentação, Engenharia Biomédica e Física da Radiação (LIBPhys-UNL), Departamento de Física, Faculdade de Ciências e Tecnologia da Universidade Nova de Lisboa, Monte da Caparica, 2892-516, Caparica, Portugal

<sup>7</sup>Associated Laboratory in Translation and Innovation towards Global Health (REAL), Monte da Caparica, 2892-516, Caparica, Portugal

Corresponding author: Lilli Anders (e-mail: lilli.anders@online.de).

**ABSTRACT** Toddlers with congenital limb deficiencies, such as fibular hemimelia, face major barriers to independent mobility during a critical window of motor development. Despite the need for early intervention, existing orthoprosthetic solutions are often inaccessible and poorly suited to the anatomical and functional needs of children aged 12–36 months. This study presents a novel, user-centered approach to a modular pediatric lower limb orthoprostheses dubbed +Limb developed in close collaboration with caregivers, physicians, and therapists. Using additive manufacturing, successive prototypes were rapidly produced and tested in a clinical setting. The final device met key requirements for modularity, light weight, postural support, and adjustability. Functional evaluations demonstrated significant improvements, including correction of a 4.5 cm leg length discrepancy, reduction of pelvic tilt from 15° to 0°, and initiation of unassisted gait with controlled knee flexion up to 45°. To study how the body and muscles responded, different sensors were used, including pressure sensors (FSRs), muscle activity sensors (EMG), and a pressure plate for foot contact analysis. This case study demonstrates the feasibility of a low-cost, customizable orthoprostheses for toddlers with fibular hemimelia and emphasizes the advantages of combining additive manufacturing and sensor-based feedback to support early-stage rehabilitation in pediatric populations.

**INDEX TERMS** Additive manufacturing, fibular hemimelia, gait analysis, pediatric orthoprostheses, user-centered design.

## I. INTRODUCTION

Walking typically emerges between 18 and 24 months of age, marking a pivotal milestone in a child's physical development [1], [2]. This achievement enhances neuromuscular coordination, balance, and postural control, laying the groundwork for future mobility and independence [1], [3]. However, children with congenital lower limb deficiencies, such as fibular hemimelia, tibial hemimelia, and congenital femoral deficiency, often face significant delays or require support to walk. These disabilities can adversely affect their quality of life, limit opportunities for motor learning, and hinder social integration, leading to increased risks of isolation and reduced participation in peer activities [4], [5]. Although individually rare, these conditions collectively impact a notable number of children worldwide.

Recent studies estimate the global incidence of Congenital Limb Reduction Defects (CLRDs) at approximately 4.48 per 10,000 live births, with regional variations observed [6]. In the United States, the prevalence of major lower limb loss in children is about 38.5 cases per 100,000, with congenital deficiencies accounting for 84% of these cases [4]. Early intervention is crucial for supporting motor development in children with limb deficiencies [7]. However, there is a significant lack of dynamic, growth-adaptive assistive solutions specifically designed for toddlers aged 12–36 months [2]. While some pediatric devices exist, they are often adaptations of adult systems intended for older children and inadequately address the rapid growth and biomechanical challenges of early childhood [8]. These solutions are often temporary and static.

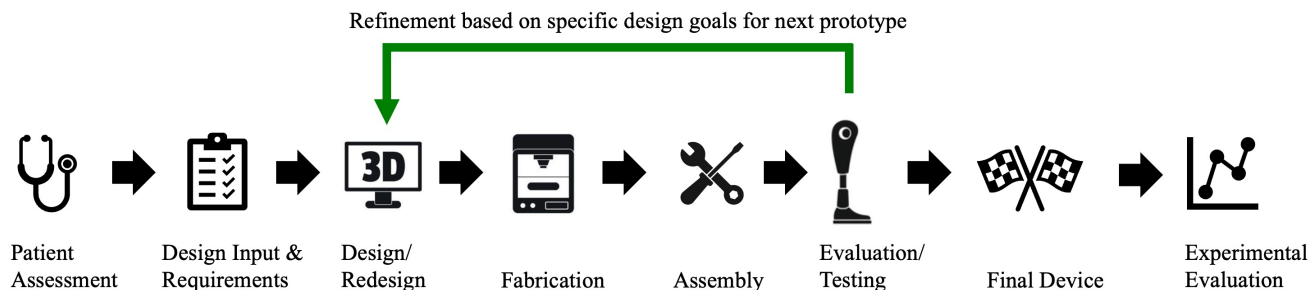


**FIGURE 1.** Global overview of the methodological pipeline used to develop the +Limb orthoprosthetic. The process began with patient assessment and definition of design requirements, followed by digital modeling, fabrication, and assembly. Prototypes were evaluated and iteratively refined based on specific design goals, culminating in a final device that underwent experimental evaluation in both hospital and home settings.

They require frequent replacement as the child grows and lack features for progressive adaptation, such as adjustable alignment, size, or support. Additive manufacturing (AM), particularly fused deposition modeling (FDM), presents an opportunity to deliver low-cost, anatomically tailored devices for early pediatric rehabilitation. Despite these advancements, fully integrated and adaptive orthotic systems for toddlers remain rare. This highlights an urgent need for orthoprosthetic solutions that accommodate physical growth while supporting early-stage motor development [8]. An orthoprosthetic is a hybrid device. It combines orthotic support, which stabilizes or corrects a limb, with prosthetic components that replace missing segments. This study introduces the first tested modular orthoprosthetic for toddlers with fibular hemimelia, made entirely through 3D printing and designed to adapt as the child grows.

## II. MATERIALS & METHODS

A global overview of the methodological pipeline used for this study is provided in Fig. 1. The development of the +Limb orthoprosthetic was carried out in close collaboration with Hospital D. Estefânia – Unidade Local de Saúde de São José. A co-creation approach was used, involving healthcare professionals, caregivers, and the engineering team throughout the process. The study followed the ethical standards of the 1964 Helsinki Declaration, and written informed consent was obtained from the child's guardians.

The process started with a patient assessment, where the child's condition was analyzed and the functional goals were defined. After this, measurements of the affected limb were taken to ensure an accurate fit. Based on these data, the design requirements were set, and a short review of materials from the literature helped identify suitable options for 3D printing.

Using these inputs, a digital model of the orthoprosthetic was created in Fusion 360. The parts were then fabricated with 3D printing, where print orientation and infill patterns were chosen according to the mechanical demands of each component. Afterwards, the printed parts were assembled and tested, both mechanically and with caregiver feedback. The design was refined through several iterations to improve strength, comfort, and usability. After each testing cycle, the

results were used to make further adjustments. This process led to the final prototype, which was evaluated for both functionality and stability in the hospital setting and later during home use.

### A. CLINICAL & FUNCTIONAL REQUIREMENT

**General Pediatric Considerations.** Toddlers present unique anatomical and biomechanical challenges that must be considered when designing orthoprosthetic devices. In early childhood, children have a high Center of Mass (CoM), a wide stance, developing muscle control, and more side-to-side movement in their upper body [9]. Their gait cycle is characterized by short, flat-footed steps, prolonged double-limb support phases, and limited energy efficiency [10], [11]. Healthy adults can recover up to 60–70% of mechanical energy during walking, largely through efficient use of passive dynamics and an optimized, pendulum-like gait. In comparison, toddlers only recover about 40% of energy because they move up and down more and their Center of Mass (CoM) and Center of Pressure (CoP) are not as coordinated [11]. As a result of this inefficiency, toddlers rely more on midfoot and forefoot loading for stability rather than the mature heel-strike and toe-off pattern seen in adult gait [12].

Fibular hemimelia (FH) is the most common birth defect that affects how long a limb is and comes with various structural and functional problems. It usually comes with differences in limb length, knee deformities that turn inward, and issues with soft tissues like missing or underdeveloped ligaments and toes. [13], [14]. According to the Paley classification system, FH can be categorized into four types based on ankle stability and joint involvement, ranging from mild to severe deformity [14]. Type 1 has a stable ankle; Type 2 has a flexible valgus deformity; Type 3 has fixed equinovalgus deformities with different levels of joint involvement (split into 3A–3C); and Type 4 has a fixed equinovarus ankle. In many cases, secondary musculoskeletal conditions, such as Knee Flexion Contracture (KFC), coexist with FH, further impairing standing posture, increasing energy demands during movement, and limiting postural transitions [15], [16]. These overlapping deformities often reduce the child's ability

to bear weight on the affected limb, delaying or preventing independent ambulation.

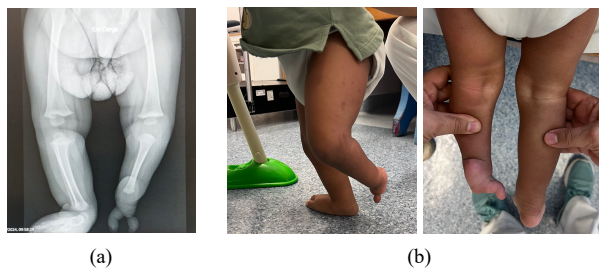


**FIGURE 2.** Clinical presentation of fibular hemimelia (Paley Type 3C). (a) Illustration of the Type 3C anatomical deformity and pre-treatment X-ray of a toddler with bilateral tibial hemimelia, showing tibial deficiency, misalignment of the knee, ankle, and foot joints, and near-complete absence of the tibiae. (b) Clinical photographs of the patient showing limb posture, leg length discrepancy, and natural standing position.

**Case-Specific Clinical Background.** This case study presents a pediatric patient diagnosed with fibular hemimelia, classified as Paley Type 3C [14]. This type includes a missing tibia and misaligned joints at the knee, ankle, and foot. These abnormalities result in a stiff foot shape and an unstable foot position. The X-ray before treatment (also Fig. 2; a) shows that the tibia is completely absent, with a significant limb length discrepancy. The ankle is misaligned, and the foot bones, including the talus and calcaneus, are missing. In the absence of this functional ankle-foot complex, it is biomechanically unviable for the child to bear weight directly through the distal tibial segment. Additionally, the outer part of the femur is underdeveloped, contributing to knee instability. Clinical examination (Fig. 2; b) revealed a flexion contracture at the knee and a crouched posture with absent heel contact, highlighting the need for stable support of the midfoot and forefoot during standing and gait initiation.

**TABLE 1.** Key functional requirements and associated KPIs.

ID	Requirement	Metric / KPI
R1	Lightweight construction	< 500g
R2	Modular and adjustable components	Yes/No
R3	Knee joint mobility support	$\geq 0-120^\circ$
R4	Correction of leg length discrepancy	$\geq 4.5$ cm
R5	Stable plantar surface	Yes/No
R6	Comfortable, ergonomic fit	Reaction of child
R7	Breathable, soft materials	Reaction of child
R8	Easy donning and doffing	$\leq 60$ s
R9	Affordability	$\leq 100$ Euro
R10	Growth adaptability	Parametrization

The orthoprosthetic was designed based on typical gait characteristics of children aged 12 to 36 months as well as the child's specific impairments to ensure the device met key functional needs (Table 1).

The orthoprosthetic was designed as a modular system consisting of an upper and lower shell, a knee section, a foot adapter, and a prosthetic foot. The design included an open foot area where the child's natural foot could rest in

its fixed equino-valgus position without being compressed. Below this, a foot adapter was added to compensate for the leg length difference and connect to the prosthetic foot, which provided a stable base for standing and walking. To compensate for the inability to bear weight through the distal tibial segment, the modular system was designed to stabilize the limb through the upper shell, broad Velcro straps and soft foam padding to distribute pressure along the surface of the limb, ensuring comfortable and secure support. Each part was made to be adjustable, allowing the orthosis to support the child's anatomy and adapt as they grow.

## B. MEASUREMENT PROTOCOL

To correctly model the components of the orthoprosthetic, precise anthropometric measurements were required. These measurements were recorded from the affected limb to ensure an anatomically tailored fit and optimal functional performance (Fig. 3). Each measurement is labeled in Fig. 3 and described in detail in Table 2. These values were critical for defining the external geometry of the prosthetic foot module and for ensuring compatibility with everyday footwear without compromising gait or stability.

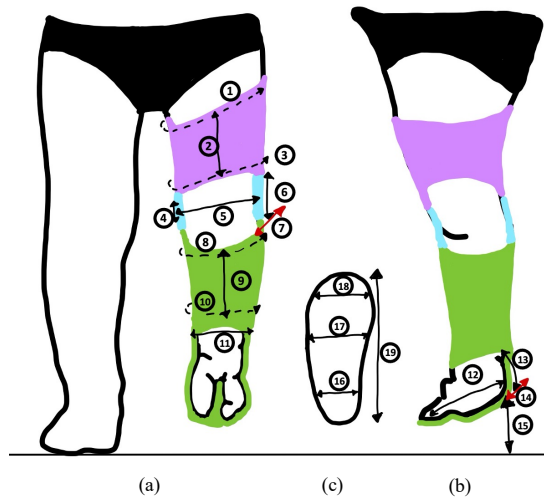


**FIGURE 3.** Anthropometric measurement protocol used to guide the orthoprosthetic design. (a) and (b) illustrate frontal and lateral views of the affected limb, highlighting segmental measurements for the upper shell (purple), knee joint alignment (blue), and lower shell (green). (c) shows plantar view measurements of the shoe sole. Dashed lines indicate circular measurements and solid lines correspond to linear segment lengths.

The toddler's body weight was also measured to accurately define loading conditions for FEA and mechanical testing.

## C. DIGITAL DESIGN WORKFLOW

This stage corresponds to the digital modeling and redesign phase of the overall workflow shown in Figure 1. Autodesk Fusion 360 was used to create the 3D models of the orthotic shells, knee joint, foot adapter, and prosthetic foot. While fully parametric modeling would have been ideal for scal-

**TABLE 2.** Numbers corresponding to Fig. 3 to clearly indicate which anatomical dimensions needed to be captured for the orthoprosthesis design process.

ID	Measurement	ID	Measurement
1	Upper thigh circumference	11	Foot width
2	Upper thigh length	12	Foot length (including toes)
3	Lower thigh circumference	13	Heel height
4	Lateral knee bone length	14	Heel width
5	Medial-lateral knee width	15	Heel-to-floor distance
6	Vertical length of knee section	16	Heel width for footwear fit
7	Depth of knee cavity	17	Midfoot width for footwear fit
8	Upper lower leg circumference	18	Toe width for footwear fit
9	Lower limb length	19	Total length of healthy foot/shoe
10	Ankle circumference		

bility, the child's irregular anatomy required manual adjustments during hospital visits. Key features such as shell length, circumference, and adapter height were defined as adjustable parameters to accommodate anticipated growth during the project period. Fit optimization was performed directly on the child, without limb casting or 3D scanning. Shell geometry, joint alignment, and interface contours were iteratively refined based on feedback from therapists and caregivers. Each design cycle involved modeling, 3D printing, assembly, and clinical evaluation, forming a continuous loop of physical and digital refinement.

**TABLE 3.** 3D printing parameters used for orthotic device fabrication.

Parameter	Value	Material	Component
Nozzle diameter	0.4 mm	PLA & TPU	All components
Layer height	0.2 mm	PLA & TPU	All components
Infill density	15% / 50% / 100%	TPU / PLA	Sole / Adapter / Shell
Printing temperature	215°C / 230°C	PLA / TPU	All PLA parts / Sole
Bed temperature	60°C / 50°C	PLA / TPU	All PLA parts / Sole
Print speed	0.20 mm/s (layer) / 40–60 mm/s (travel)	PLA & TPU	All components
Cooling fan speed	100% / Off or low	PLA / TPU	All PLA parts / Sole
Print orientation	Flat / horizontal	PLA & TPU	All components
Printing pattern	Gyroid / Grid / Rectilinear	TPU / PLA	Sole / Adapter / Shell

#### D. MATERIAL SELECTION & 3D PRINTING PARAMETERS

Material selection for this project prioritized practicality, safety, and adaptability to rapid prototyping. The goal was to support the clinical design and evaluation of the orthotic device, rather than conducting extensive materials research. The choices were based on recent studies about 3D printing that show which materials work best for orthotic and prosthetic uses [17]–[20].

Three main materials were used: Polylactic Acid (PLA), carbon fiber-reinforced PETG (PETG-CF), and Thermoplastic Polyurethane (TPU). Table 4 summarizes their key mechanical properties, which were also used as direct inputs for FEA conducted after the final prototype was built (shown in Sec. III-D). PLA reinforced with carbon fiber (PLA-CF) is also discussed in the literature as a potentially stronger alternative to standard PLA [18]. However, this study focused on comparing one standard material, such as PLA, with

one carbon-fiber-reinforced material. PETG-CF was chosen instead of PLA-CF because it showed better strength and stiffness in earlier research [17], [18]. Both PLA-CF and PETG-CF have potential drawbacks, including increased brittleness and reduced interlayer bonding strength, which are particularly critical in dynamic, load-bearing applications for pediatric use.

**TABLE 4.** Mechanical properties of 3D printed materials used in FEA simulation.

Property	TPU (95A Shore)	PLA	PETG-CF
Young's modulus (GPa)	0.004	3.500	5.000
Poisson's ratio	0.38	0.39	0.35
Density (g/cm <sup>3</sup> )	1.20	1.300	1.300
Tensile yield strength (MPa)	10.000	49.500	60.000
Tensile ultimate strength (MPa)	12.000	50.000	75.000

Fabrication was performed using FDM. Multiple prototypes were produced to evaluate the influence of print parameters, including infill percentage, internal pattern, and print orientation. PLA was used especially during the development of modular components and for most prototypes because of its low cost and ease of printing. It showed high print success rates, a low risk of cracking, and was ideal for rapid iterative development. PETG-CF was initially considered for the final device due to its high stiffness, tensile strength, and favorable strength-to-weight ratio [17], [18], [20]. It also outperformed PLA in preliminary FEA simulations (Sec. III-D). Its carbon fiber reinforcement improved rigidity while reducing density. Despite reports of brittleness and poor interlayer adhesion in the literature, these studies primarily focused on adult or heavier patients. Therefore, we assumed that the lower impact forces generated by toddlers could lessen the severity of these limitations in practice. However, during testing of the prototype, PETG-CF still showed signs of breaking easily, especially at the joints that lined up with the direction of the print layers, which is explained further in Section V. TPU was selected for the sole to mimic soft tissue behavior and shock absorption in the human foot. The final functional prototype used a combination of PLA and TPU.

Table 3 summarizes the optimized parameters used in the final working prototype. All components were printed with a 0.4 mm nozzle and a 0.2 mm layer height, settings shown to provide a good compromise between detail and mechanical strength [21], [22]. Printing temperatures were set to 215°C for PLA and 230°C for TPU. Bed temperatures were 60°C and 50°C, respectively. Cooling fans were used at 100% for PLA and turned off or set low for TPU to ensure bonding and prevent warping. Infill density was adjusted based on functional requirements. Load-bearing parts like the knee joint and lower shell used 100% infill. The foot adapter, which was less likely to fail under load, was printed with 50% infill to reduce material use and overall weight without significantly compromising stiffness [23]. The sole, which required compliance, was printed at 15% infill. These choices were

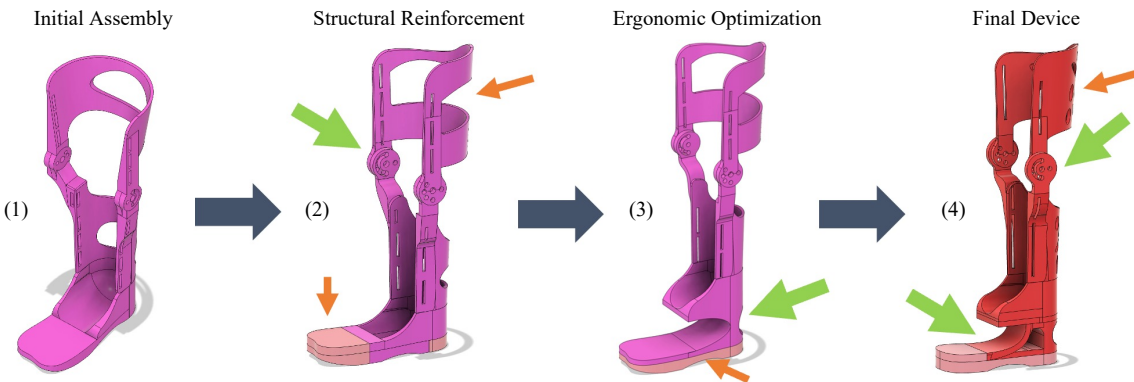


**FIGURE 4.** Evolution of the orthoprosthetic device across four prototype iterations. Major refinements are shown with green arrows including structural reinforcement of the knee joint and redesign of the foot adapter. Minor refinements are shown with orange arrows, including the use of TPU components and adjustments to the shell shape. The process led to the final device, which was used for clinical evaluation.

guided by mechanical performance data, including ASTM D638 tensile tests [21], [24]. Different infill patterns were applied by region: gyroid for flexibility in the sole, grid for the adapter, and rectilinear in rigid structures. All parts were printed in a flat orientation to enhance inter-layer bonding [21] and improve stability against shear forces generated by the child's leg during movement.

The completed device remained functional and structurally intact during a three-week testing period. All materials used are widely accepted for biomedical prototyping and are considered safe for noninvasive pediatric applications.

### III. DESIGN PROCESS

The design process for the orthoprosthetic device followed an iterative and modular approach, beginning with the individual development and testing of critical components. Rather than constructing the complete orthoprosthetic device from the outset, the project prioritized the isolation and optimization of key functional elements, such as the knee joint mechanism, foot structure, and the upper and lower shells. Each component was individually designed, 3D-printed, and tested to assess anatomical fit and structural integrity. This modular strategy enabled early identification of design flaws and technical challenges, laying a solid foundation for full integration. The user-centered feedback cycle also helped to ensure that the prototypes not only met clinical and biomechanical goals but were also practical and comfortable for daily use.

Following successful validation of the individual components, a pre-prototype was assembled using manually joined parts. The knee joint was temporarily affixed to the upper and lower shells using a mechanical press-fit technique. Although this configuration did not provide sufficient structural stability for dynamic functional testing, it effectively served to assess spatial alignment between the different components. Based on this preliminary evaluation, the components were subsequently printed as an integrated prototype, allowing the first real-world tryouts with the child. All prototypes from the first to the final are shown in Fig. 4.

#### A. INITIAL ASSEMBLY

The first assembly features a two-part shell system, with an upper thigh shell and a lower calf-foot shell connected by a mechanical knee joint. This joint consists of interlocking elements on either side, joined by a central pivot to allow limited flexion and controlled movement. Along the vertical length of both shells, multiple rectangular slots were incorporated to accommodate 1.5cm wide Velcro straps, enabling adjustable and secure fastening tailored to the user's anatomy. The design includes material-reduced areas, such as cut-outs in the posterior thigh and calf regions, intended to reduce weight (Fig. 4, (1)). The footplate is printed as a single rigid element, shaped to follow the natural foot contour but lacking any integrated soft zones or cushioning. Overall, this prototype focused on basic structural functionality.

#### B. STRUCTURAL REINFORCEMENT

Building on feedback from the first prototype, the second iteration introduced enhanced structural support, particularly in the upper shell near the knee region, to improve the stabilization of the child's knee during movement. The knee joint system received a major structural revision to address limitations observed in the initial prototype. Originally, the joint featured a bulky surrounding structure that restricted motion and was prone to early mechanical failure. To improve flexibility and durability, the structural bulk was reduced. The updated design included more robust, non-printed pins, replacing the weaker printed ones to improve stability. Additionally, the pinholes and overall joint surface area were slightly enlarged to address these problems. A dual-pin system was introduced, consisting of one stop pin and one guiding pin positioned on opposite sides of the joint (Fig. 4, (2)). Together, these pins controlled how far the joint could move at specific angles of 0°, 45°, 90°, and 110°, allowing for smooth and balanced movement (Table 1; R3). The knee supports connecting to the shells were redesigned with rounded edges. Sharp corners in the original version had caused instability in the simulations. Rounding the edges improved strength and stress distribution.

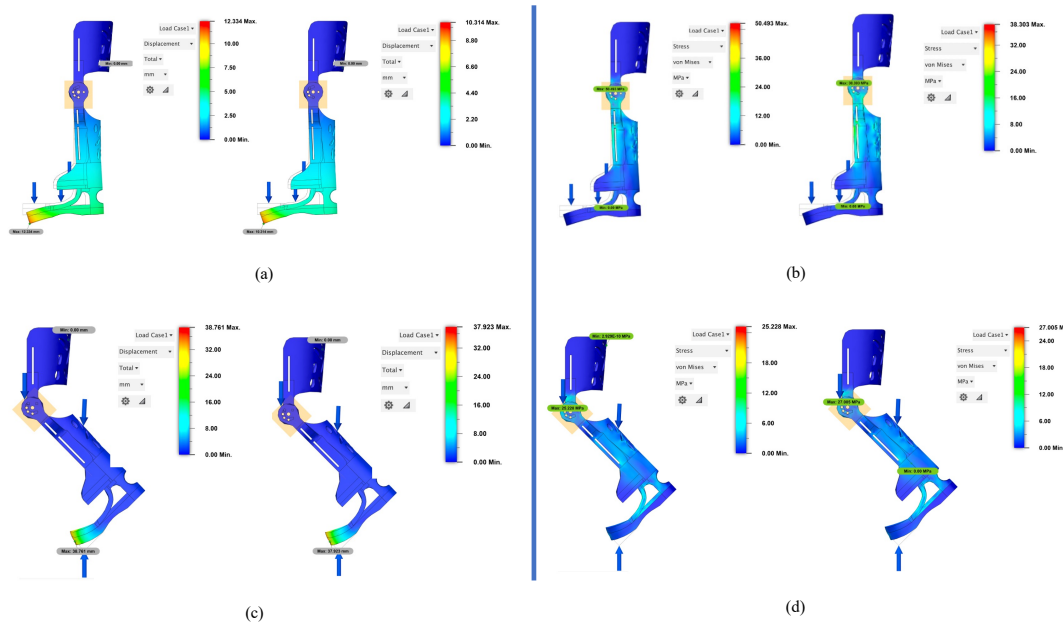


**FIGURE 5.** FEA analysis comparing PLA (left) and PETG-CF (right) orthosis models, both simulated with a TPU sole and toe section. (a) Displacement under standing posture; (b) von Mises stress under standing posture; (c) Displacement in a flexed-knee ( $45^\circ$ ) position; (d) von Mises stress in the  $45^\circ$  flexed-knee position. Simulations show greater overall displacement in the TPU sole and toe region, while PETG-CF exhibits more even stress distribution and reduced peak stress compared to PLA.

The strapping system was further optimized by replacing the multiple narrow 1.5 cm straps with fewer, wider 2.5 cm straps, improving overall stability for the child's leg as well as the movement within the orthosis. TPU was added to the toe and heel sections to improve shock absorption, ensuring a more natural and less rigid gait.

#### C. ERGONOMIC OPTIMIZATION

This third prototype introduces a key structural refinement to address the limb length discrepancy. The natural foot contour is extended downward via a smoothly integrated height adapter, which transitions into the prosthetic foot base. This dual-foot structure includes an upper section that preserves the anatomical shape of the user's residual foot and a lower prosthetic segment that compensates for the vertical height difference between limbs (Fig. 4, (3)). This approach allows for a more balanced, aligned standing position and improves gait symmetry (Table 1; R4). The entire lower segment, including the adapter and prosthetic foot was printed as a single piece. The sole underneath was entirely made of TPU, offering flexibility for gait and improved surface grip. To improve wearability, the foot section was reshaped to better fit inside a standard shoe, including a carved-out area at the heel to make insertion of the prosthetic foot easier. Material around the knee area was more closely contoured to the child's anatomy.

#### D. FINAL DESIGN

For the final device, FEA was conducted to compare the performance of PLA and PETG-CF after some design refinements were made.

The height adapter was first redesigned as a modular, screw-on component. The new version mimics the shape of the natural foot counter using a 1 cm-thick plate with two screw holes. Beneath this plate, a central support structure shaped like a slide was added, extending downward into the prosthetic foot to provide additional stability and load distribution. The screw holes of the adapter and foot counter enabled precise control over both inward and outward rotational movement of the prosthetic foot (Fig. 4, (4)). It also enabled the use of additional adapter plates to incrementally adjust the device in response to the child's growth (Table 1; R2).

Both the upper and lower shells were redesigned to provide increased surface coverage for enhanced support. Ventilation holes were added to keep the device breathable and light with providing additional support (Table 1; R7). The strapping system was also upgraded, using wider 5 cm Velcro straps lined with thick neoprene to maximize limb stability within the device and help offload pressure from the tibia.

Finally, the heel section was further reduced, while additional material was added to the forefoot to improve stability in the shoe and weight transfer during walking. Additional TPU material was applied to the toe area, increasing flexibility and contributing to a more natural and fluid gait (Table 1; R5). This design was then simulated with FEA.

**Mechanical Evaluation through FEA** The simulations were performed using Autodesk Fusion 360 with a static stress study. A model-based tetrahedral mesh was applied, with automatic element sizing and a refinement level set to approximately 3% of the overall part scale. This procedure

resulted in a moderately fine mesh capable of capturing deformation in complex geometries such as the prosthetic foot and joint region. The upper shell of the orthoprosthetic was fully fixed to replicate its attachment to the residual limb.

Two loading scenarios were simulated to assess mechanical performance: vertical static loading and an inclined 45° load representing the toe-off phase of walking. Each simulation compared the two material configurations for the orthoprosthetic: PLA and PETG-CF, as mentioned in Section II-D. In both configurations, the sole and toe section were modeled using TPU, selected for its elastic and cushioning properties to mimic a more natural gait pattern.

All materials were modeled as linear, elastic, and isotropic, with mechanical properties listed in Fig. 4. It is important to note that while TPU was included in the model to reflect its intended structural role, its mechanical behavior was simplified as a linear elastic material due to the limitations of the Fusion 360 solver. The software does not support nonlinear or viscoelastic simulations with large deformations, which are required to realistically simulate TPU's time-dependent and nonlinear response under load. As a result, displacement values in the TPU region should be interpreted qualitatively rather than quantitatively. However, because TPU was modeled identically in both configurations, relative differences in structural response between PLA and PETG-CF remain valid and informative. This limitation is acknowledged and further discussed in Section V.

A load of 200 N was applied vertically to the plantar surface in the static loading scenario. Based on the study by Nilsson and Thorstensson [25], peak vertical ground reaction forces (vGRF) during walking can reach up to 1.5 times body weight. For a child weighing 11 kg (approximately 108 N), this corresponds to a peak vGRF of:

$$F = 1.5 \times 108 \text{ N} = 162 \text{ N}$$

To account for dynamic and unpredictable movements typical of children, a safety buffer was applied and approximated the required load capacity to 200 N. This approach ensures a sufficient representation of the forces acting on the orthosis during functional use. For the inclined load case, the same 200 N force was applied at a 45° angle to the toe region to simulate the toe-off phase of gait.

In the vertical static displacement analysis (Fig. 5; a), the PLA + TPU configuration exhibited a maximum displacement of 13.33 mm, primarily located in the TPU portion of the prosthetic foot adapter, which extends beneath the natural foot shell to compensate for limb length discrepancy. The toe region of the adapter displayed the highest deformation, shown in orange to red tones, while the midfoot area exhibited green to yellow, indicating moderate displacement. Additionally, light green shading reached into the base of the rigid PLA structure, particularly in the lower part of the natural foot shell, suggesting that some of the load-induced movement was transferred beyond the TPU zone into the stiffer material.

In contrast, the PETG-CF + TPU configuration showed a reduced maximum displacement of 10.14 mm. In this case, the deformation remained more tightly localized within the forefoot section of the TPU adapter, with blue to green coloration dominating the rest of the shell, indicating minimal movement. The PETG-CF upper structure remained largely rigid, demonstrating improved load containment and allowing the TPU to function more effectively as a compliant interface. Although the displacement values in the TPU region are not predictive due to modeling simplifications, this difference in deformation pattern reflects each material's ability to stabilize the flexible base.

The von Mises stress analysis (Fig. 5; b) showed that both configurations had similar highest stress values: 38.35 MPa for PLA and 38.30 MPa for PETG-CF. However, while the absolute stress values were nearly identical, their significance differs when considered relative to each material's mechanical capacity. PLA typically has a tensile strength of approximately 50 MPa, meaning the observed stress approached its lower failure threshold, especially given PLA's brittle nature and poor fatigue resistance. In contrast, PETG-CF has a higher tensile strength of approximately 70 MPa. Therefore, the PETG-CF configuration remained well within its safe operating limits, offering a greater mechanical buffer and reduced risk of structural failure under repeated loading. Stress was primarily concentrated around the central joint region in both cases, but PETG-CF distributed these forces more evenly, reducing the likelihood of localized failure or fatigue.

Under walking conditions simulated with a 45° inclined load (Fig. 5; c), both configurations experienced higher total displacements due to the combined axial and bending forces. The PLA + TPU model reached a maximum displacement of 38.76 mm, slightly higher than the 37.92 mm observed for the PETG-CF + TPU setup. As with the vertical loading case, the largest displacements occurred in the TPU region. While these values are exaggerated due to linear modeling, the trend remains consistent: PETG-CF limited the spread of deformation more effectively than PLA. In the PETG-CF configuration, displacement was more tightly concentrated in the TPU toe region, indicated by a compact green-to-yellow gradient. In contrast, the PLA model showed more spread-out deformation, with a broader transition of color gradients extending into surrounding regions. Such behavior suggests that load was transferred further into the structure in the PLA model, while PETG-CF more effectively contained the deformation within the intended flexible zone. This indicates that PETG-CF provides greater stiffness and shape retention, contributing to overall orthosis stability under dynamic loading.

Finally, stress analysis under the walking scenario (Fig. 5; d) showed a peak of 25.23 MPa in the PLA model and 27.01 MPa in the PETG-CF model. Despite the slightly higher stress, the PETG-CF configuration remained mechanically safe due to its superior material strength and fatigue resistance. In contrast, the PLA structure approached its perfor-

mance threshold, posing a higher risk of long-term failure under cyclic loading. Further interpretation of these findings and real-world testing outcomes are discussed in Section V. Based on the simulation results, the prototype was initially printed in PETG-CF. However, its performance did not match the simulated behavior, so the same design with slight improvements was reprinted in PLA for the final device.

To prevent mechanical failure of the knee joint, the final design was proactively reinforced. Prior iterations consistently exhibited structural weaknesses in the knee area. In response, the joint's surface area was enlarged, and material was added around key stress concentrations, particularly between the mounting holes and along the guiding slot. These changes enhanced both the volume and mechanical stability of the joint interface. Additionally, the inner and outer joint components were reversed in the final design, improving alignment and enabling a more even distribution of loads during movement. The final device combined these improvements into a user-ready model.

#### IV. RESULTS

The results are organized into four subsections, each corresponding to a distinct phase of the orthoprosthesis evaluation. The first subsection focuses on static postural alignment and pelvic symmetry during quiet standing to assess structural correction, combining visual observation with quantitative data from force platform analysis. The second subsection presents observations from early unassisted walking trials, highlighting functional adaptation, gait initiation, and initial force-sensitive resistor (FSR) data to characterize step timing and loading asymmetry. The third subsection includes temporally normalized electromyography (EMG) recordings to evaluate repeatable patterns and muscle activation in the lower leg muscles.

The final subsection reports findings from a controlled treadmill-based gait cycle analysis conducted under therapist supervision. This structure clearly demonstrates how the device influences biomechanical support and motor learning during early stages of independent mobility.

##### A. STATIC ALIGNMENT AND PELVIC CORRECTION

This subsection evaluates the static postural alignment and pelvic symmetry with and without the orthoprosthesis during quiet standing, using both visual observation and quantitative assessment via force platform analysis.

Fig. 6 illustrates the child's postural alignment across three conditions: (a) standing without orthoprosthesis, (b) upright posture with manual support but no orthotic assistance, and (c) aligned stance while wearing the orthoprosthesis.

In the unloaded condition without the orthoprosthesis (Fig. 6; a), the child exhibited a marked leg length discrepancy of 4.5 cm, resulting in significant pelvic tilt of around 15° toward the affected side. This asymmetry was accompanied by lateral displacement of the hip center, indicating compromised pelvic control and asymmetric loading.

The affected limb showed valgus deviation and medial ro-

tation, contributing to visible misalignment of the lower extremities. In the absence of a structured plantar support surface, weight was borne primarily on the lateral and dorsal aspects of the foot, leading to further destabilization. A compensatory shift in the CoP toward the unaffected limb was evident, reducing the capacity to engage the shorter side in stable weight-bearing. This postural imbalance likely increases the risk of secondary complications such as asymmetric gait development or spinal curvature.

Support by the therapist (Fig. 6; b) enabled the child to achieve a more upright posture, but it did not correct the underlying biomechanical asymmetries. Pelvic tilt and limb misalignment persisted, and independent stable standing or walking was not possible without external support.

When fitted with the custom 3D-printed orthoprosthesis, several key postural improvements were observed (Fig. 6; c). The device effectively compensated for the leg length discrepancy, restoring pelvic symmetry as indicated by the leveling of the iliac crest. The hip axis appeared re-centralized, contributing to improved axial alignment and upright stance. The affected limb followed a straighter mechanical axis, reducing angular deviation and improving load-bearing alignment with the body's centerline. The prosthetic foot provided a stable and flat plantar surface, facilitating full-foot contact and more equal load distribution between limbs. Notably, the CoP was observed in a more central position when the orthoprosthesis was worn, suggesting enhanced postural stability and greater readiness for bipedal gait initiation.

In addition to these visual postural improvements, center of pressure (CoP) was assessed using the PLUX 1D force platform, which features four independent steel load cells arranged equidistantly beneath a 450 × 450 mm aluminum plate. By analyzing the vGRF forces distributed across its quadrants, the platform enables precise computation of CoP and offers quantitative insight into weight distribution and balance behavior during quiet standing. Fig. 7 provides a multi-part view of the pressure plate. Panel a illustrates the quadrant layout of the plate, divided into Q1–Q4, representing the forefoot and rearfoot regions of each foot. Panel B shows the child standing on the pressure plate while wearing the orthoprosthesis during a 60-second data acquisition period. Clear bilateral foot placement is observed, allowing for direct comparison between the affected and non-affected sides. The child positions the prosthetic foot slightly more anteriorly and does not fully align it with the right foot. This misalignment may partially account for the higher pressure signal observed in Q1 compared to Q4 (Panel c).

However, it is also possible that the child is actively shifting more weight onto the forefoot of the prosthetic limb as a compensatory strategy to enhance balance and postural control during standing. Previous studies have indicated that the absence of an anatomical ankle joint can lead to increased anterior loading on the prosthetic side [26], [27]. Panel c displays the pressure signal output across all quadrants over time. The temporal pattern is similar across all quadrants, likely due to subtle postural sway while standing. This data

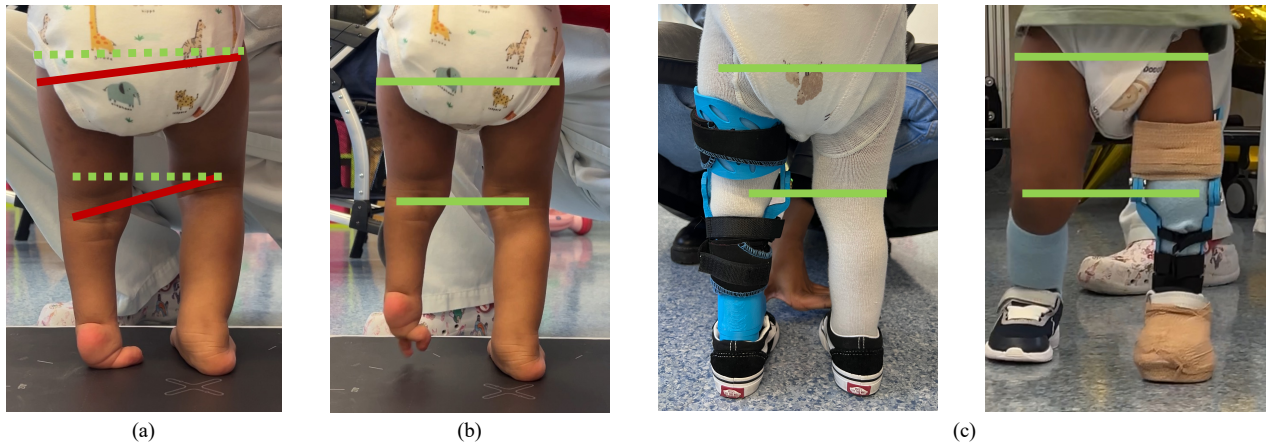


**FIGURE 6.** Postural alignment and limb positioning before and after orthotic intervention. In each image, dotted lines indicate the intended or ideal alignment, while solid lines represent the observed orientation of body segments. (a) Standing without orthoprosthetic support, showing significant pelvic tilt and lack of stable foot positioning. (b) Child being manually supported into an upright position without any assistive device, demonstrating inability to maintain alignment or initiate gait independently. (c) Properly fitted orthoprosthetic support supporting improved pelvic alignment, corrected leg positioning, and enabling standing and walking without external assistance.

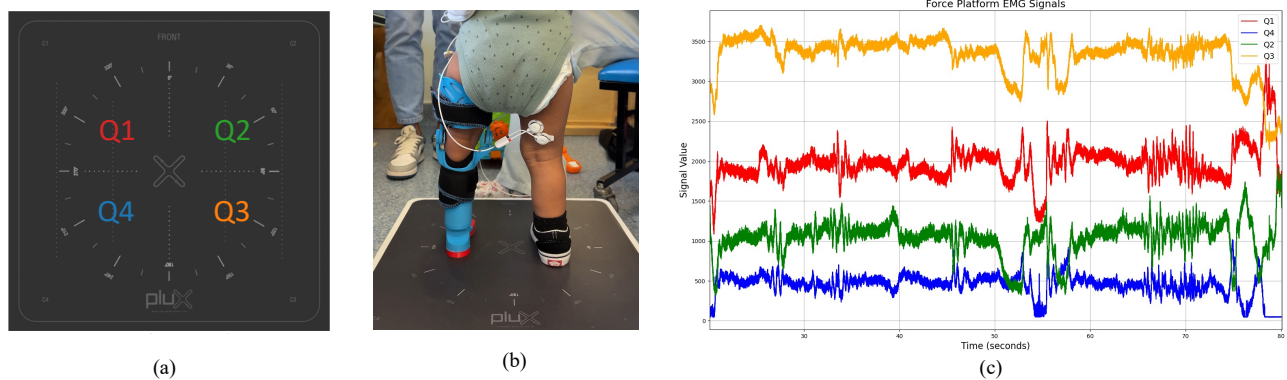


**FIGURE 7.** Plantar pressure distribution assessment using a quadrant-based pressure plate. (a) Top view of the pressure plate divided into four quadrants (Q1–Q4) for measuring load distribution. (b) The child standing on the plate during testing, with slight misalignment of the feet relative to the plate's center. (c) Pressure data recorded over a 60-second period, showing asymmetrical weight distribution across quadrants, with consistently higher loading in Q3 and Q1.

is a positive indication that the child is able to engage both legs in a coordinated manner to maintain balance, suggesting early postural control and the ability to hold a stable position despite the weakness on the left side. However, the magnitude of pressure differs notably between quadrants, indicating uneven weight distribution between the limbs.

To better understand the uneven weight distribution between the legs, the data were visualized using a box-and-whisker plot (Fig. 8; a), which shows the range and variation in vGRF from each foot while the child was standing. The plot shows that the right foot supports significantly more force, with a mean of 34.82 N compared to 14.81 N on the left. This results in an absolute difference of 20.01 N and a relative asymmetry of 40.3%, meaning about 58.4% of the total weight is carried by the right foot. The right foot also has a higher median and a wider spread of values, indicating greater total load and more variation in how the force is

applied. In contrast, the left foot shows less force overall and a narrower range, but still contributes in a steady and consistent way. Even though this imbalance is clear, the fact that there is consistent force on the left foot shows that the weaker leg is actively involved, which is a positive sign of early motor control. A Wilcoxon signed-rank test confirmed that the difference is statistically significant ( $p < 0.000001$ ), meaning it is unlikely to be due to chance. Considering the physical and neural adjustments required for standing with a new support device, this force pattern may reflect a functional compensation strategy. Overall, these results suggest that the child is already using both legs to maintain balance, showing signs of early postural control and a strong potential for continued recovery and development.

Fig. 8; b displays the CoP trajectory, offering an additional perspective on the child's postural control strategy during early standing. In this plot, X = 0 cm marks the midline of

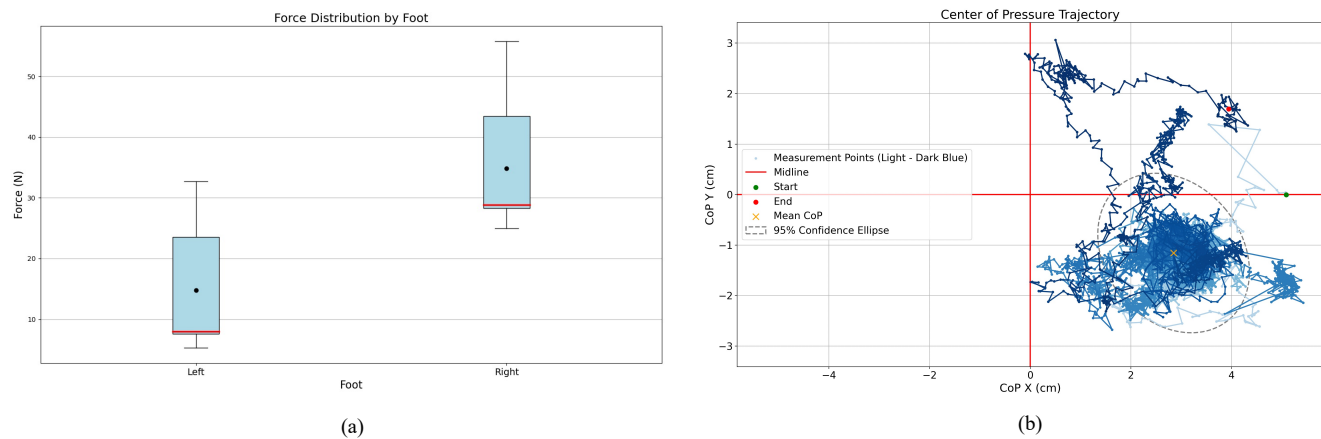


**FIGURE 8.** (a) Showing the distribution of vGRFs under each foot during early standing. The right foot exhibits significantly higher and more variable force, indicating an asymmetric load distribution with greater reliance on the unaffected limb. Black dots indicate the median values, while red horizontal lines represent the mean. (b) CoP trajectory plotted in x and y plane. The CoP path, shown as a color gradient from light to dark blue (early to late), starts at the blue dot and ends at the green dot. The CoP is clustered in the rear-right quadrant, suggesting a rearfoot-biased and rightward stance. The red cross marks the mean CoP location, and the dashed purple ellipse denotes the 95% confidence area.

the plate, separating left and right foot positions. The CoP trajectory, shown as a gradient from light to dark blue, indicates the temporal progression of pressure shifts, with lighter lines marking early movement and darker lines representing later stages. The trajectory is densely clustered between -1 and -2 cm on the Y-axis, revealing a rearfoot-biased stance. While it is typical for toddlers to distribute weight toward the rear of both feet during early standing, in this case, the CoP is centered almost exclusively over the right foot, indicating an asymmetric reliance on the unaffected limb. This pattern still reflects a normal early postural strategy, favoring stability through rearfoot loading, but highlights the child's compensatory use of the right leg for most of the support. This variation is consistent with findings by Pourreza et al. [28], who noted that toddlers often adopt a posterior weight shift as part of typical postural development. The CoP is also concentrated around 2–3 cm on the X-axis, indicating a rightward weight shift. This suggests that while the left foot maintains ground contact, it contributes only slightly to load-bearing, in agreement with the force asymmetry observed in Fig. 8; a. The start point and end point further illustrate that the CoP remained predominantly in the right-rear quadrant throughout the observation period.

Occasional anterior shifts of the CoP are also visible, indicating transient balance corrections. These limited dynamic forward excursions likely indicate that the child is making early attempts at reactive postural adjustments to maintain upright stability. The mean CoP position and 95% confidence ellipse confirm that most of the movement remains localized in the rear-right quadrant, with only brief excursions away from this zone.

Overall, these findings demonstrate that the orthoprosthesis significantly improves postural alignment, promotes partial functional loading of the affected limb, and facilitates

early-stage bilateral stance, even if asymmetrical, laying a critical foundation for further motor and neural development.

#### B. EARLY UNASSISTED WALKING BEHAVIOR

This subsection aimed to evaluate whether the orthoprosthesis could support unassisted walking, facilitate early gait initiation, and ensure acceptance of the device by the toddler by also analyzing gait patterns with FSR sensors.

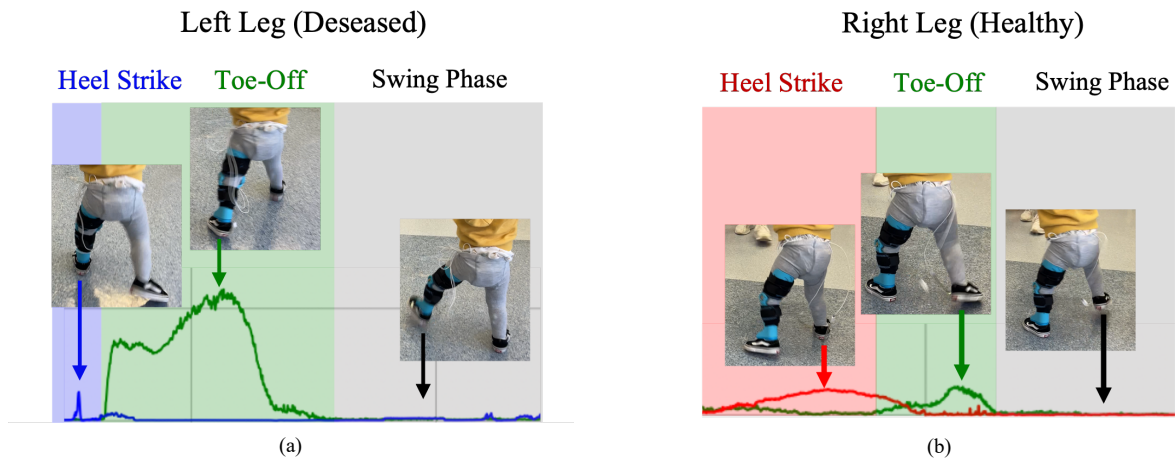
After completing the postural assessment, the orthoprosthesis was tested during early walking trials. Remarkably, the child was able to initiate walking almost immediately without external support and adapted comfortably to the device.

Fig. 9 shows early unassisted walking with the orthoprosthesis in a clinical hallway. The child used wide arm movements, forward trunk sway, and cautious weight shifts. These patterns help maintain balance by widening the base of support and adjusting step timing [29]. Arm abduction and forward reach suggest a reliance on proprioceptive and vestibular input. This type of behavior is common in toddlers, as postural control and trunk stability are still developing [29]. While precise control of the orthotic knee had not yet been established, the child was able to initiate step sequences, shift weight onto the prosthetic side, and maintain upright posture. During walking, the affected leg tended to move outward, reflecting the child's ongoing learning process and incomplete understanding of how to actively control knee flexion and extension. The knee bent about 45°, which matched the limits of the prosthetic device, but the timing and control of the bending were inconsistent, which is normal for someone still learning to walk.

To capture plantar pressure during walking, two FSR sensors were affixed underneath the shoe soles of both legs, one positioned under the heel and the other beneath the forefoot, near the medial side of the big toe. The sensors were taped to stay in place during gait. The heel sensor detected heel-strike



**FIGURE 9.** Sequential images showing early, unassisted walking attempts with the 3D-printed orthoprosthetic. The child demonstrates forward trunk sway, wide arm movements, and cautious weight shifting.



**FIGURE 10.** Gait analysis of early unassisted walking. (a) Left leg demonstrates successful but less smooth phase transitions, reflecting developing motor control and prosthetic adaptation. (b) Right leg shows clear transitions through heel strike, toe-off, and swing phase, with corresponding FSR sensor activation patterns.

events, while the forefoot sensor captured toe-off phases during the gait cycle. This is shown in Fig. 10 which presents the FSR sensor activation profiles alongside video stills for both legs in a full gait cycle, focusing on the three key phases of walking: heel strike, toe-off, and the swing phase. The right leg (a) shows a typical gait pattern for a toddler. Heel strike is smooth and well-controlled, with a gradual rise in force indicating stable weight acceptance. Toe-off is sharp and clearly defined, reflecting strong propulsion. During the swing phase, the leg unloads properly, with minimal activity as it moves forward. Despite being affected by FH, the left leg (b) still demonstrates a complete gait cycle. Heel strike is brief, with only a small spike in activity, suggesting reduced heel contact and a shift toward forefoot loading. Toe-off is longer and broader, indicating a more effortful push-off, likely a compensatory strategy for limited strength or motor control. The transition into the swing phase is slightly delayed but clearly present, with the leg properly unloaded.

### C. EXPLORATORY EMG ANALYSIS DURING UNASSISTED GAIT

To evaluate neuromuscular coordination and functional symmetry between the affected and unaffected limb, surface EMG signals were recorded using BioPlux wireless sensors placed on the gastrocnemius (GC) and tibialis anterior (TA) muscles of both legs, which are essential in walking. Signals were sampled at 1000 Hz, converted to millivolts, and rectified. A 50 ms moving RMS window was used to extract the signal envelope, and data were segmented and time-normalized across four gait cycles to assess muscle activation timing and variability. The shaded areas representing  $\pm 1$  standard deviation across the different trials (Fig. 11).

On the left leg, the TA displayed elevated EMG amplitudes and substantial inter-cycle variability. This pattern suggests compensatory overactivation, likely due to the limited contribution of the antagonist muscle group during stance and the child's effort to stabilize the ankle during swing. Correspondingly, the RMS curve for the left TA shows a consistently elevated profile, further emphasizing the increased muscular effort required on the affected side. In contrast, the right TA

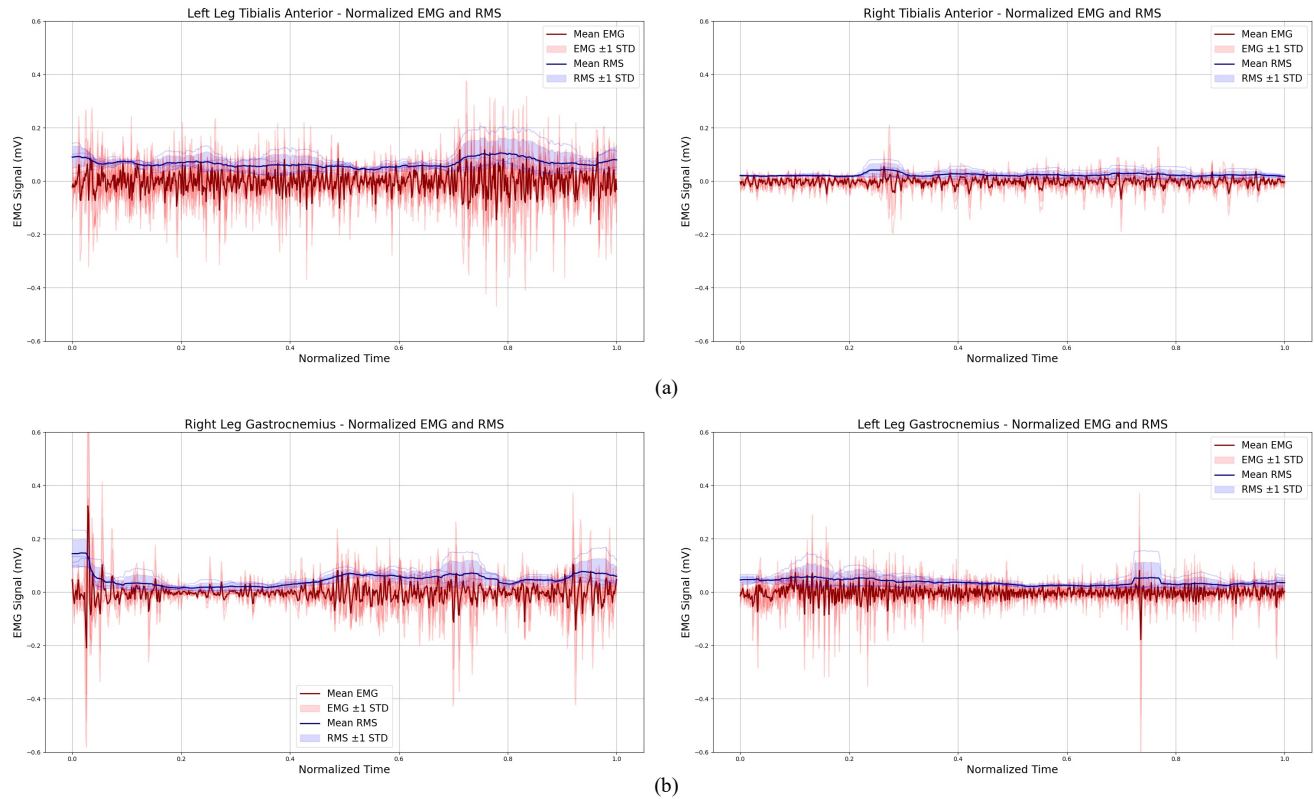


**FIGURE 11.** Temporally normalized surface EMG and RMS signals of the TA (a) and GC (b) muscles on the left (affected) and right (unaffected) legs across four gait cycles during unassisted walking. Red curves represent the mean EMG with  $\pm 1$  standard deviation, and blue curves show RMS with variability. All signals are in millivolts (mV), plotted on a unified y-axis for comparison. The left TA shows elevated, variable activation, consistent with compensatory dorsiflexor overuse. The left GC presents reduced but patterned activation. Right leg muscles exhibit stable, phase-appropriate recruitment. Results highlight asymmetrical motor strategies and early neuromuscular engagement of the prosthetic limb.

exhibited a more stable and phase-appropriate activation pattern, with a distinct peak at heel strike and lower variability. The right leg's GC showed well-defined activation during push-off, indicating effective plantarflexion control. The low standard deviation suggests consistent recruitment across gait cycles.

The left GC demonstrated markedly reduced activity and a relatively flat RMS profile, confirming minimal engagement of this muscle during gait. This shows the movement problems linked to FH and indicates that the muscles on the affected side are not working together properly. These findings show that the child uses a different approach with their muscles, relying more on the front muscles of the left leg while using the calf muscles less.

The RMS analysis adds to the raw EMG by giving a clearer picture of how much effort the muscles are using, which helps explain the lack of use and the compensating actions in the affected limb.

This result indicates that the neuromuscular pathways are functional and responsive. While current limitations in strength and coordination are evident, the presence of muscle activation provides a promising outlook. Continued use of the orthoprosthesis along with targeted walking practice and

therapy could lead to gradual improvements in muscle control and balance, showing great promise for recovery in the long run.

#### D. CONTROLLED GAIT CYCLE ON A TREADMILL

To validate and extend the findings from unassisted walking trials, a controlled treadmill assessment was conducted under therapist supervision using the final orthoprosthesis. This evaluation focused on the repeatability and coordination of gait patterns, with particular attention to orthotic knee function. Fig. 12 presents a time-sequenced image series of the treadmill trial. The upper sequence (a) illustrates the motion of the healthy limb during a complete gait cycle, while the lower sequence (b) shows the orthoprosthetic side. Both limbs demonstrate consistent and comparable phase transitions, including initial contact, stance, toe-off, and swing. This picture is suggesting that the child has internalized a basic motor pattern for gait and is able to actively coordinate the orthotic knee with the natural limb. In this structured setting, the movements appeared more rhythmic, indicating early motor learning consolidation. Notably, the child consistently achieved approximately  $45^\circ$  of controlled orthotic knee flexion during swing, matching the joint's mechanical limit

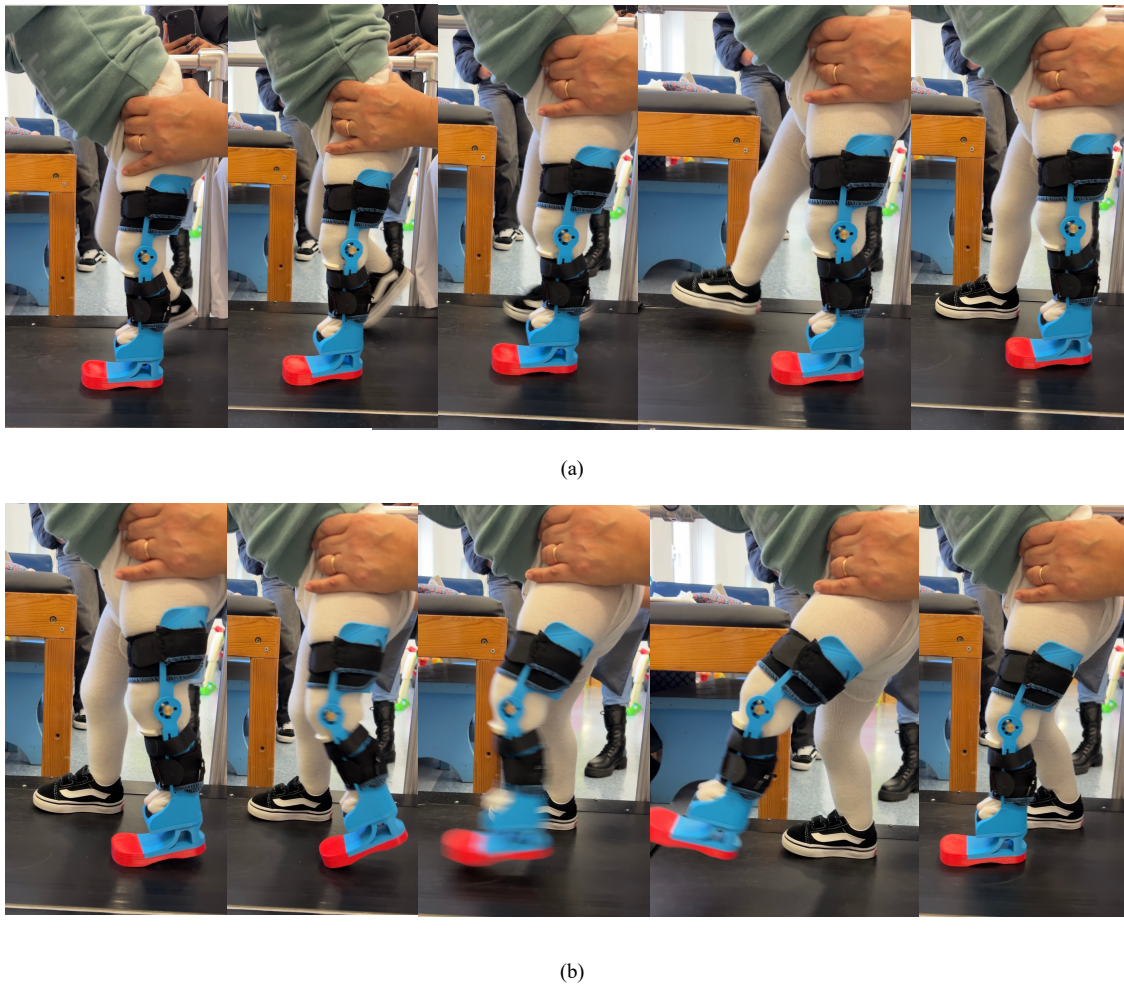


**FIGURE 12.** Comparison of gait patterns between the healthy limb (a) and the orthoprosthetic limb (b) during treadmill walking. Both sequences demonstrate similar motion phases (stance, swing, toe-off), indicating that the child developed functional control of the orthotic knee. The orthoprosthetic device supports coordinated movement and dynamic load transfer during early walking.

and reflecting successful adaptation. The TPU outsole and reinforced toe section contributed to flexible ground contact and rollover, which aids mid-stance progression and weight transfer; these design features were discussed earlier.

Together, these findings confirm that the orthoprosthetic device supports not only spontaneous gait initiation but also repeatable, coordinated movement in a controlled environment. The treadmill setting further reinforced step rhythm and helped the child refine motor control, demonstrating the device's capacity to support safe and progressive gait training.

## V. DISCUSSION

This study highlights the functional impact and technical feasibility of a custom 3D-printed orthoprosthetic device in supporting early standing and gait development in a toddler with FH. Clinically, the device corrected leg length discrepancy and pelvic asymmetry, enabling bilateral stance and improved

postural alignment. Even though the weight was still uneven and favored the healthy leg, the pressure and center of pressure data showed that the child was starting to coordinate their posture with both legs. Early unassisted walking further demonstrated the prosthesis's ability to support functional gait initiation. Compensatory strategies such as trunk sway and wide arm movements were observed, aligning to early development patterns in toddlers. Gait phase transitions were evident on both limbs. EMG data confirmed active muscle recruitment, even in the affected limb, despite neuromuscular imbalances. The consistent overactivity of the TA, along with early use of the plantarflexors, indicates a pattern of motor learning that the prosthesis helps to support. Further analysis of temporally normalized EMG and RMS signals revealed coordinated activation across all four muscles. The left TA showed higher and inconsistent EMG and RMS readings, which aligns with overuse as a compensatory response for

dorsiflexion. In contrast, the right GC showed stable and phase-appropriate plantarflexor recruitment. Although the left GC demonstrated reduced activation, its RMS profile still followed a recognizable gait-phase pattern, indicating emerging functional use. The active recruitment of all four muscles confirms that the prosthetic limb was functionally engaged rather than passively carried. These findings suggest that continued use of the prosthesis, supported by gait training, may promote more balanced, efficient activation patterns over time. This muscle activity is also likely to gradually move the CoP more towards the prosthetic side, helping to balance the weight better while standing. The prosthesis's ability to support coordinated orthotic knee motion during treadmill trials further confirms its utility in enabling realistic early-stage gait patterns. Although the child demonstrated immediate acceptance of the device and initiated unassisted walking, sensor-based data confirmed that full functional loading of the affected limb was not yet achieved. This limitation is attributable to the child's underlying anatomy. Due to the absence of the foot and ankle bones, and a short, soft-tissue-covered tibial segment, direct distal weight-bearing was mechanically unfeasible at this stage. Consequently, the current design did not function as a traditional socket-type prosthesis. Instead, it employed a distributed load strategy using wide contact surfaces and padded strapping to stabilize the limb. As the child matures and the musculoskeletal structure develops, future iterations of the device will incorporate more socket-like characteristics to improve surface contact and pressure distribution, supporting safer and more balanced weight transfer during gait.

In parallel to the clinical findings, this study also evaluated the mechanical and material behavior of the orthoprosthesis under pediatric-specific loading conditions. Initial FEA simulations guided material selection, favoring PETG-CF for its low predicted displacement and stress levels, supported by prior studies highlighting its rigidity and strength-to-weight ratio [17], [18], [20]. However, real-world testing revealed a discrepancy between simulated and actual performance: PETG-CF prototypes failed during early dynamic use due to joint fractures along layer lines. This result was consistent with its known anisotropic and brittle behavior in 3D-printed applications [18], [20].

In contrast, PLA, despite showing higher stress and deformation in simulation, proved more robust during clinical testing. Its good layer bonding and balanced stiffness allowed it to withstand the mechanical demands of toddler gait over a three-week test period without structural failure.

Although the final prototype withstood the three-week evaluation period without structural failure, the long-term effects of cyclic loading and material fatigue remain a concern. Toddlers exhibit variable movement patterns and repetitive loading, which can accelerate wear in high-stress regions such as the knee joint and shell interfaces. PLA provided acceptable short-term durability, but its fatigue resistance is lower than that of high-performance polymers. Over extended use, this may lead to cracks or delamination at critical points,

particularly along layer lines common in FDM-printed components.

To address this, the device was intentionally designed with modularity in mind. All components are interchangeable, enabling straightforward part replacement without requiring full device reprinting. This approach not only enhances maintainability but also supports rapid adaptation as the child grows or as specific components degrade. Future work will focus on exploring alternative materials with improved fatigue performance and establishing guidelines for routine inspection and replacement of modular components. Additionally, long-term studies under real-life conditions are needed to confirm the durability of the modular design and optimize replacement intervals to ensure sustained safety and function.

TPU, used in the sole and toe sections, played a key role in cushioning and gait adaptation. In simulation, it showed the highest deformation especially in the forefoot during toe-off. While this reflects its flexible role in the design, the result should be interpreted with caution due to the use of a simplified linear elastic model. The large displacement initially raised concerns about TPU being too soft for stable support. However, this behavior aligns with its known ability to mimic the soft tissue under the foot, helping to smooth ground contact and push-off. To achieve the desired balance between flexibility and stability, different infill densities and printing patterns were tested experimentally, allowing the final TPU design to offer effective energy absorption without compromising structural integrity. Its durability under repeated loading, supported by prior studies on 3D-printed foot prosthesis, further contributed to comfort and reduced stress at the foot-ground interface.

Beyond materials, the iterative prototyping approach allowed for refinement of mechanical features such as the knee joint, shell geometry, and open foot design. These adjustments helped accommodate equino-valgus posture and allowed for modular growth adaptation. A defining strength of this project was its co-creation methodology, which actively involved physiotherapists, physicians, and caregivers throughout the design process.

This project addresses a gap in pediatric assistive technology, where most existing studies focus on older children or utilize rigid, non-modular systems. For instance, Mansilla Navarro *et al.* [2] demonstrated effective motion assistance using soft exosuits but did not address congenital limb deficits or 3D-printed customization. Similarly, traditional Knee Ankle Foot Orthosis-based case studies in older children [30] lack considerations for early developmental stages or low-cost production methods.

The present findings therefore contribute novel clinical and technical evidence supporting the use of fully 3D-printed, modular orthoprosthetic solutions for toddlers with congenital limb differences. Importantly, the divergence between simulation predictions and real-world outcomes reinforces the need for dynamic validation under real-use conditions. While computational tools remain valuable in early design phases, they must be paired with user-centered testing to

ensure safety, durability, and clinical efficacy.

In addition to clinical performance, qualitative feedback from the child's caregivers highlighted important aspects of day-to-day usability. The final prototype was described as easy to don and doff, with the wide Velcro strap system enabling quick adjustments and a secure fit. Caregivers also noted that the device was well-tolerated during extended wear periods, with no observed skin irritation or pressure marks. These insights underscore the importance of comfort and convenience in pediatric orthotic design, particularly in early rehabilitation stages where caregiver compliance is critical.

Finally, this work demonstrates the potential of combining additive manufacturing, participatory design, and rapid prototyping into a scalable framework, particularly relevant for low-resource settings, where access to pediatric orthotic care remains limited.

## VI. CONCLUSION

This study presents the first documented clinical evaluation of a low-cost, 3D-printed, user-centered orthoprostheses specifically developed for toddlers with FH. The +Limb device met its key design objectives, demonstrating functional effectiveness, anatomical adaptability, and comfort during early gait initiation.

As summarized in Table 1, the final prototype successfully met most design requirements (R1–R9). It corrected a 4.5 cm leg length discrepancy (R4), enabled unassisted gait with 45° knee flexion (R3), improved pelvic alignment from 15° tilt to 0° (R5), and maintained a lightweight, modular, and comfortable fit (R1, R2, R6). Additionally, caregivers reported that the device was easy to use and convenient to put on and take off (R8). These outcomes confirm the functional and clinical relevance of the proposed device. The low material cost further supports its applicability in both high-resource and resource-constrained healthcare environments. Nonetheless, the breathability of the system (Table 1, R7) was limited, primarily due to the use of soft padding on the inner surfaces of the shells. Furthermore, no temperature measurements were conducted to quantitatively assess this limitation. A fully parametrized version fulfilling (Table 1, R10) has not yet been realized and will need further adaptation in future prototypes.

Although this study involved a single case, it reflects established practice in exploratory medical device research, where detailed single-subject trials serve as critical first steps toward broader clinical validation. The design and testing methodology presented here is replicable and provides a practical foundation for future studies involving larger pediatric patients. While this single-case design is typical in exploratory device testing, future work should include larger, longitudinal trials to validate scalability and durability across a broader pediatric population.

Limitations of this study should be acknowledged. The short evaluation period precluded assessment of long-term durability, fatigue resistance, and adaptation to varied environmental conditions. The prototype was tested in a toddler with relatively low muscular strength, and its suitability for

older children with more advanced motor demands remains uncertain. Additionally, the current design lacks mechanical damping, which could improve impact absorption and joint stability during high-load activities such as stair climbing or jumping. Another relevant aspect for future work would be the use of more advanced solvers for FEA to better capture the nonlinear behavior of materials such as TPU and enhance predictive accuracy in future design iterations.

Data collection also presented challenges. Although several recordings were made, sensor discomfort and detachment reduced the quantity of usable qualitative data. To achieve more accurate and generalizable conclusions, particularly regarding the longitudinal development of muscle control and motor coordination, larger and more complete datasets will be required, ideally collected over an extended period. Future work will aim to create orthoprostheses with built-in sensors that can monitor walking in real-time and adjust automatically, while ensuring the sensors are comfortable and stay in place. Such integration could improve both data accuracy and user compliance, allowing for continuous, child-friendly monitoring of biomechanical and neuromuscular function during daily use.

The +Limb project exemplifies how low-cost, personalized technologies can challenge conventional care models and advance equitable access to pediatric rehabilitation, particularly for very young children currently underserved by commercial orthotic solutions. This proof of concept demonstrates that affordable, customized orthoprosthetic care for toddlers is achievable, potentially transforming early rehabilitation in resource-constrained healthcare settings.

## ACKNOWLEDGMENTS

The authors would like to thank the participating child and their family for their trust, time, and cooperation throughout this study. Special thanks are extended to the clinical team at Hospital de Dona Estefânia, Lisbon, for their support during the evaluation process and for providing access to clinical facilities.

The authors gratefully acknowledge Professor Bruno Soares for his invaluable guidance, technical expertise, and mentorship during the design and testing phases. This work was carried out with the support of Instituto Superior Técnico, NOVA School of Science and Technology (NOVA-FCT), and the 3D Printing Lab for Health, whose infrastructure and collaboration were essential to the development of this project.

This project was partially funded by FCT/MECI through national funds and, when applicable, co-funded EU funds under project UID/50008: Instituto de Telecomunicações. This work was also funded by Fundação para a Ciência e Tecnologia (FCT, Portugal) through national funds UI/BD/151321/2021 (LIBPhys-UNL) and LA/P/0117/2020 (REAL).

## REFERENCES

- [1] K. E. Adolph and S. R. Robinson, "The road to walking: What learning to walk tells us about development," in *Advances in Child Development and*

- Behavior* (J. Benson, ed.), vol. 48, pp. 1–40, Academic Press, 2015.
- [2] P. M. Navarro, D. Copaci, and D. B. Rojas, “Design and control of a soft knee exoskeleton for pediatric patients at early stages of the walking learning process,” *Bioengineering*, vol. 11, no. 2, p. 188, 2024. Open Access under CC BY 4.0.
- [3] M. H. Woollacott, “Postural control and aging,” *Handbook of Clinical Neurology*, vol. 17, no. 3, pp. 219–231, 1998.
- [4] L. M. Hart, T. L. Miller, and T. Craig, “Lower limb loss in children: Epidemiology and health care utilization in the united states,” *PM&R*, vol. 12, no. 5, pp. 423–430, 2020.
- [5] N. Jones, P. Black, and L. Tran, “Incidence of congenital limb deficiencies: A systematic review,” *Journal of Limb Loss Research*, vol. 4, no. 2, pp. 45–56, 2021.
- [6] S. Tan, M. Ochieng, and L. Ahmed, “Limb reduction defects: Global patterns and trends based on who database analysis,” *International Journal of Pediatric Research*, vol. 11, no. 1, pp. 12–19, 2023.
- [7] H. Gerber, D. Cho, and N. Patel, “Neurodevelopmental outcomes and early intervention in children with limb deficiencies,” *Developmental Medicine and Child Neurology*, vol. 62, no. 3, pp. 324–331, 2020.
- [8] M. Sarajchi, M. K. Al-Hares, and K. Sirlantzis, “Wearable lower-limb exoskeleton for children with cerebral palsy: A systematic review,” *IEEE Transactions on Neural Systems and Rehabilitation Engineering*, 2021.
- [9] W. Liu *et al.*, “Biomechanical characteristics of the typically developing toddler: A narrative review,” *Frontiers in Pediatrics*, vol. 10, p. 8946917, 2022.
- [10] B. Bril, A. Ledebt, E. Berton, *et al.*, “Kinematics in newly walking toddlers does not depend upon postural stability,” *Journal of Neurophysiology*, vol. 94, no. 3, pp. 1832–1842, 2005.
- [11] T. D. Ivanova, V. Gritsenko, L. B. Popova, *et al.*, “Mechanical energy in toddler gait: a trade-off between economy and stability?”, *Journal of Experimental Biology*, vol. 207, no. 14, pp. 2417–2426, 2004.
- [12] K. M. Whitcome, N. B. Holowka, and D. E. Lieberman, “Ontogenetic changes in foot strike pattern and calcaneal loading during walking in children,” *Journal of Experimental Biology*, vol. 220, no. Pt 19, pp. 3565–3573, 2017.
- [13] R. C. Hamdy, A. M. Makhdom, N. Saran, and J. G. Birch, “Congenital fibular deficiency,” *Journal of the American Academy of Orthopaedic Surgeons*, vol. 22, no. 4, pp. 246–255, 2014.
- [14] C. B. Fuller, C. E. Shannon, and D. Paley, “Lengthening reconstruction surgery for fibular hemimelia: A review,” *Children*, vol. 8, no. 6, p. 467, 2021. Open Access.
- [15] A. Bartonek and C. Lidbeck, “Knee flexion while walking exceeds knee flexion contracture in children with spastic cerebral palsy,” *Children*, vol. 10, no. 12, p. 1867, 2023.
- [16] D. C. Kerrigan *et al.*, “Crouched posture maximizes ground reaction forces generated by the legs,” *Journal of Biomechanics*, vol. 45, no. 9, pp. 1679–1684, 2012.
- [17] M. Daly, M. Tarfaoui, M. Bouali, and A. Bendarma, “Effects of infill density and pattern on the tensile mechanical behavior of 3D-printed glycolylized polyethylene terephthalate reinforced with carbon-fiber composites by the FDM process,” *Journal of Composites Science*, vol. 8, no. 4, p. 115, 2024.
- [18] J. Rybarczyk, F. Górski, W. Kuczko, R. Wichniarek, S. Siwiec, N. Vitkovic, and R. Pácurar, “Mechanical properties of carbon fiber reinforced materials for 3D printing of ankle foot orthoses,” *Advances in Science and Technology Research Journal*, vol. 18, no. 4, pp. 191–215, 2024.
- [19] M. Pastorino, F. Galli, L. Gastaldi, and M. Vidoni, “Numerical and experimental mechanical analysis of additively manufactured ankle–foot orthoses,” *Applied Sciences*, vol. 12, no. 17, p. 8650, 2022.
- [20] P. Steck, D. Scherb, C. Witzgall, J. Miehling, and S. Wartzack, “Design and additive manufacturing of a passive ankle–foot orthosis incorporating material characterization for fiber-reinforced PETG-CF15,” *Materials*, vol. 16, no. 9, p. 3503, 2023.
- [21] M. N. Ahmad, M. R. Ishak, M. Z. Zulkafle, *et al.*, “The effect of Fused Deposition Modeling parameters (FDM) on the mechanical properties of Polylactic Acid (PLA) printed parts,” *Journal of Advanced Research in Applied Mechanics*, vol. 123, no. 1, pp. 238–246, 2024.
- [22] H. Chokshi, D. B. Shah, K. M. Patel, and S. J. Joshi, “Experimental investigations of process parameters on mechanical properties for PLA during processing in FDM,” *Advances in Materials and Processing Technologies*, 2021.
- [23] T. J. Coogan and D. O. Kazmer, “Infill effects in 3D printed parts under tensile and impact loads,” *Additive Manufacturing*, vol. 16, pp. 172–179, 2017.
- [24] M. S. Chaudhry and A. Czekanski, “Evaluating fdm process parameter sensitive mechanical performance of elastomers at various strain rates of loading,” *Materials*, vol. 13, no. 14, p. 3202, 2020.
- [25] J. Nilsson and A. Thorstensson, “Ground reaction forces at different speeds of human walking and running,” *Acta Physiologica Scandinavica*, vol. 136, no. 2, pp. 217–227, 1989.
- [26] F. Miller, J. Slade, R. Montgomery, G. Lipton, and R. Marks, “Weight distribution of below-knee amputee and able-bodied children during standing,” *IEEE Transactions on Rehabilitation Engineering*, vol. 3, no. 4, pp. 366–370, 1995.
- [27] L. Brady, K. R. Kaufman, L. Vrbos, D. Fish, and D. Levinson, “Standing pressure distribution for normal and below-knee amputee children,” *Journal of Prosthetics and Orthotics*, vol. 1, no. 3, pp. 152–157, 1989.
- [28] E. Pourreza, S. Jalali, S. Ostadbaba, A. Aguiar, D. Barone, F. Silva, I. Da Cunha, V. Zatsiorsky, and M. Latash, “Spatiotemporal evolution of toddlers’ regional foot pressure distribution and center of pressure at antero-posterior axis during learning of standing,” *Journal of Biomechanical Engineering*, vol. 146, no. 1, p. 011001, 2024.
- [29] C. N. Burnett and E. W. Johnson, “Development of gait in childhood: Part ii,” *Developmental Medicine & Child Neurology*, vol. 13, no. 2, pp. 207–215, 1971.
- [30] R. Raj, A. Dixit, K. Łukaszewski, R. Wichniarek, J. Rybarczyk, W. Kuczko, and F. Górski, “Numerical and experimental mechanical analysis of additively manufactured ankle–foot orthoses,” *Materials*, vol. 15, no. 17, p. 6130, 2022.



**LILLI ANDERS** is an early-career researcher holding a Bachelor of Science in Business Informatics from Leuphana University. Prior to her graduate studies, she gained practical experience through internships in robotics and web development. She is currently pursuing her master's degree in Biomedical Engineering and in Robotics & Intelligent Systems at Instituto Superior Técnico in Lisbon. Since 2024, she has been engaged in interdisciplinary research at the 3D Printing Center for Health, NOVA School of Science and Technology (FCT NOVA), with a focus on medical device innovation. Her current research interests include medical device design, signal processing, and the development of intelligent sensing systems for biomedical applications.



**CLÁUDIA QUARESMA** holds a PhD in Biomedical Engineering and is an Assistant Professor at NOVA School of Science and Technology – FCT NOVA. She is a full member of the LIB-Phys Research Center and the Associated Laboratory REAL. She currently serves on the Scientific Council of FCT NOVA, the Evaluation and Quality Council of the Polytechnic Institute of Beja as an external member, and the Scientific Council of the Alcoitão School of Health as an invited member. In addition, she coordinates the 3D Printing Center for Health. She is the author of several scientific articles and book chapters and is also a patent holder. Over the past five years, she has coordinated approximately 45 projects in collaboration with hospitals and companies and has received 14 awards in the areas of science, teaching, and innovation. Her main research interests lie in biomechanics and the development of new technologies, with a particular focus on rehabilitation.



**PAULA AGULHEIRO** holds a Bachelor's degree in Physiotherapy from the Escola Superior de Tecnologia da Saúde de Lisboa (1990) and later completed an additional degree in Physiotherapy at the Escola Superior de Saúde de Setúbal (2005), along with a postgraduate specialization in Neurodevelopmental Treatment (2002). She is currently a part-time guest assistant professor at the Escola Superior de Saúde de Setúbal, Instituto Politécnico de Setúbal, where she has also served as an instructor in the international course "BLIP – Challenges of the Future in Pediatric Rehabilitation." Professionally, she is a specialist physiotherapist at the Physical Medicine and Rehabilitation Service of Dona Estefânia Hospital, part of the Unidade Local de Saúde São José. With over three decades of experience in Pediatrics since 1991, her recent clinical focus has been on musculoskeletal disorders, particularly lower limb deformities in children and adolescents. She has also been actively involved in research and development projects related to assistive devices for children with lower limb disorders, collaborating with NOVA FCT through the 3D Printing Center for Health, and with the Biomechanics of Movement research group at the Department of Mechanical Engineering of Instituto Superior Técnico.



**HUGO PLÁCIDO DA SILVA** (Senior Member and Distinguished Lecturer, IEEE) is an award-winning biomedical researcher, inventor, and entrepreneur. He holds a PhD in Electrical and Computers Engineering, and an Habilitation title in Biomedical Engineering, both from Instituto Superior Técnico (IST) – University of Lisbon (UL). Hugo is a researcher at Instituto de Telecomunicações (IT) since 2004 and a professor at IST-UL since 2019. In addition, he is co-founder of multiple technology-based companies in the field of biomedical engineering. His work has been widely recognized at both national and international levels. His current interests include biomedical instrumentation, biosignal processing, and artificial intelligence in health, areas in which he holds 10 patents and has performed pioneering theoretical, methodological, and technical contributions.